

Numerical Investigation of Progressive Collapse of a Multispan Continuous Bridge Subjected to Vessel Collision

Hua Jiang, A.M.ASCE¹; Junjie Wang²; Mi G. Chorzepa, M.ASCE³; and Jidong Zhao⁴

Abstract: Multispan continuous bridges have been widely used in navigable waterways. However, their susceptibility to progressive collapse as a result of vessel collision is not yet fully understood. Experimental studies of bridge collapses induced by vessel collision are costly, time-consuming, and often not feasible. This paper presents a numerical study on the progressive collapse of a multispan continuous bridge subjected to vessel collision. A high-fidelity finite-element model of a 14-span continuous bridge, including its prestressed concrete (PC) superstructures and reinforced concrete (RC) pier columns/piles, and the colliding barge was developed to investigate the bridge failure mechanism. The validation was carried out for PC superstructures and RC structural members of the bridge piers by using available drop-weight impact tests of PC and RC beams. Furthermore, evaluation of available forensic investigation data, such as photographs and a survey of collapsed spans/piers, indicated that the progressive collapse was well predicted by the numerical analysis. Results show that the bridge pier directly impacted by a vessel will fail in the lateral direction of the bridge span, whereas nonimpacted piers will fail in the longitudinal direction of the bridge span. Results also show that the number of collapsed spans/piers depends on underwater terrain conditions and that the failure of the slender pier columns and piles results from plastic-hinge bending. DOI: 10.1061/(ASCE)BE.1943-5592.0001037. © 2017 American Society of Civil Engineers.

Author keywords: Vessel collision; Continuous bridges; Progressive collapse; Finite-element analysis.

Introduction

With the rapid increase in the use of vessels for transportation and the number of bridges spanning across busy navigable coastal and inland waterways, the occurrence of vessel collisions with bridges is becoming more frequent. In some cases, the collision accidents result in damage to the bridge-protection system, such as fender systems (Jiang and Chorzepa 2015a, 2016). However, there have been many instances in which bridges did not have protection systems, and vessel collision resulted in bridge damage or collapse. Harik et al. (1990) analyzed 79 bridge failures that occurred in the United States from 1951 to 1988 and reported that approximately 24% of the failures were caused by a vessel collision. Worldwide, 31 major bridge collapses caused by a vessel collision were reported from 1960 to 2002, which claimed 342 lives (AASHTO 2009). For example, a ballasted 35,000-DWT bulk carrier collided with an unprotected main pier column of the Sunshine Skyway Bridge crossing Florida's Tampa Bay in 1980. This collision accident resulted in a 396-m-long collapse of three main spans and 35 civilian deaths (AASHTO 2009). A more recent accident occurred at the Jiujiang

Bridge over the Xijiang River in Guangdong, China, in 2007, where a collision of a fully loaded 3,000-DWT sand barge damaged four roadway spans and three piers, plunging them into the river and claiming 9 lives (People.cn 2007). Vessel-bridge collision poses a serious threat to public safety, port operations, motorist traffic, and environmental protection (e.g., fuel leak) and thus has drawn increasing attention from bridge designers, transportation agencies, and the general public.

Generally, vessel-bridge collision simulations involve a highly complicated nonlinear dynamic analysis process. The accident usually happens within a few seconds, with an enormous collision-induced lateral force transmitted from an impact area to the other components of a bridge, such as bridge piles and superstructure. Cross-disciplinary knowledge in impact mechanics, bridge structural mechanics, fluid mechanics, and geomechanics are required to comprehensively understand the impact response. In spite of the fact that there have been a few experimental tests on vessel-bridge collisions in the past (Consolazio et al. 2002, 2005), various constraints limit experimental approaches. That is, full-scale tests are costly, time-consuming, and oftentimes not feasible. Reduced-scale model tests in the laboratory are often constrained because of scaling effects in structural geometry (Chu and Zhang 2011; Sha and Hao 2013a). In dealing with these difficulties, in particular, contact-based finite-element (FE) methods may offer a reasonable and practical alternative, although a considerable amount of time is required to develop a finite-element analysis (FEA) model of the colliding vessel. For example, Consolazio and Cowan (2003) used *ADINA* to develop a FEA model in which a jumbo hopper barge collided with circular and square-shaped pier columns to investigate the static force-deformation relationship of a barge bow. Similar simulations for a tanker barge against circular and square-shaped pier columns using *LS-DYNA* were reported thereafter (Consolazio et al. 2009). Consolazio et al. (2002) carried out a FE study using *LS-DYNA* to predict the magnitude of impact forces, which can be used to characterize the loading expected from the forthcoming full-scale barge-bridge impact testes (Consolazio et al. 2005). Sha and Hao (2013b)

¹Associate Professor, Key Laboratory for Bridge and Tunnel of Shannxi Province, Chang'an Univ., Xi'an 710064, China (corresponding author). E-mail: huajiang2006@hotmail.com

²Professor, State Key Laboratory of Civil Engineering for Disaster Reduction, Tongji Univ., Shanghai 200092, China. E-mail: jjqxu@tongji.edu.cn

³Assistant Professor, College of Engineering, Univ. of Georgia, Athens, GA 30602. E-mail: chorzepa@uga.edu

⁴Associate Professor, Dept. of Civil and Environmental Engineering, Hong Kong Univ. of Science and Technology, Clear Water Bay, Hong Kong. E-mail: jzhao@ust.hk

Note. This manuscript was submitted on June 7, 2016; approved on December 5, 2016; published online on February 16, 2017. Discussion period open until July 16, 2017; separate discussions must be submitted for individual papers. This paper is part of the *Journal of Bridge Engineering*, © ASCE, ISSN 1084-0702.

investigated barge collisions with a circular pier of a three-span continuous-girder bridge at three different impact velocities and compared the impact force and maximum pier displacement using *LS-DYNA*. Yuan and Harik (2008) introduced an elastoplastic spring-mass model for an analysis of collisions of multibarge flotillas with bridge piers, and the analysis results correlated well with the *LS-DYNA* simulations. Jiang et al. (2012a) modeled a collapse of a reinforced concrete (RC) bridge induced by vessel collision and identified potential failure mechanisms of the bridge structures.

Most of the existing numerical studies on vessel-bridge collisions have focused primarily on the impact behavior, such as impact force-time histories, including the peak value and impact duration. The displacements of bridge piers and the vessel-bow crush depth during the impact have been studied in some cases. Simplified FE models (e.g., mass-spring-damper model) and empirical equations of impact force have been proposed to evaluate the impact response of bridge structures against colliding vessels because the force-time history (applied as node forces on the bridge members) analysis can be completed much faster than a vessel impact analysis explicitly solved with a bridge structure. For example, design-oriented FE tools such as *FB-MultiPier* have been employed to study the barge impact response of the single bridge pier (Consolazio and Cowan 2005) and multi-piers with the superstructure (Consolazio and Davidson 2008), where the barge was represented by a force-deformation spring model with a single-degree-of-freedom lumped mass, which was coupled to the multiple-degrees-of-freedom bridge model developed by means of beam, shell, and spring elements. Furthermore, the bridge failures under quasi-static and dynamic loads resulting from vessel collisions were investigated using the same code (Davidson et al. 2010, 2013), where the failure of bridge members was considered as plastic-hinge bending failure with many plastic hinges formed in beam elements (e.g., piles, piers) under the combined action of axial load and biaxial bending moments. The FE analysis assumed that sufficient shear resistance was present in the bridge members, and thus no shear failure would occur by such vessel collision. In addition, the shock spectrum for bridges subjected to vessel collision was proposed by Fan and Yuan (2012), Cowan (2007), and Cowan et al. (2015), in which the simplified interaction analysis of vessel-bridge collision was employed.

Although these efforts to develop simplified analysis methods provide useful information for bridge design and rehabilitation against vessel collision, the simplified methods may not be sufficient to investigate the shear-induced failure of bridge members or collapse process of a bridge. The progressive collapse of a multispan

continuous bridge subjected to vessel collision is of particular interest because of its practical relevance. For example, the collision accident involving the Jiujiang Bridge in China in 2007 resulted in a progressive collapse of four spans along with three piers, despite the fact that only one pier was struck by an aberrant barge.

This study aimed to investigate the progressive collapse mechanism of the multispan continuous bridge based on the explicit nonlinear FE program *LS-DYNA* (version 971) and the official forensic investigation results of a 14-span continuous bridge (Jiang 2011). A three-dimensional (3D) FE model was developed for the vessel collision analysis and included a barge, a bridge with 14 piers and spans, and the riverbed surface. Prior to the vessel-bridge collision analysis, a validation of bridge components subjected to impact forces was completed using the available drop-weight impact test results of a RC beam (Fujikake et al. 2009) and a prestressed concrete (PC) beam (Kelly 2011).

To capture the progressive collapse mechanism caused by the vessel collision in the FEA model, a newly calibrated elastoplastic damage concrete constitutive model, MAT 145, was used in the numerical analysis (Jiang and Zhao 2015). The steel reinforcement elements in bridge structures were linked to concrete elements by *CONSTRAINED_LARANGE_IN_SOLID. The preload on concrete structures resulting from prestressing force and gravity was applied using a dynamic relaxation method, prior to an explicit vessel-bridge collision analysis, and the convergence of the dynamic relaxation analysis was defined by the *CONTROL_DYNAMIC_RELAXATION option (LSTC 2010). In addition, nonlinear P-Y springs (BSI 2010) were used to model the lateral soil-pile interaction at the riverbed. The simulations presented herein aim to demonstrate the effectiveness of the proposed FE approach for investigating the progressive failure of a multispan continuous bridge subject to vessel collision. The findings from the present study will be beneficial for future design or strengthening of similar continuous bridges to reduce the risk of progressive collapse in the event of a vessel collision.

Relevant Information for the Progressive Collapse of a Multispan Continuous Bridge

Design Information for a 14-Span Continuous Bridge

Jiujiang Bridge connects the Jiujiang town of Foshan and the Shaping town of Heshan (China) and is a part of national highway No. 325, as shown in Fig. 1. The bridge is 15.5 m wide, including a



Fig. 1. Location of Jiujiang Bridge

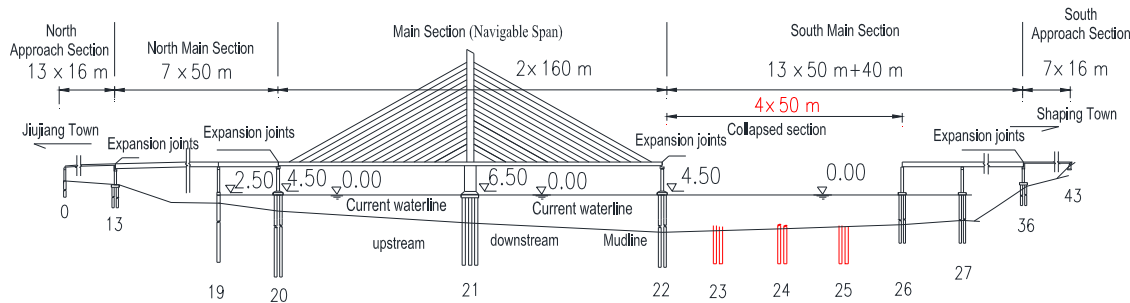


Fig. 2. Elevation of Jiujiang Bridge between Pier No. 19 and Pier No. 27 after the collision accident (unit: m)

14-m-wide carriageway with two 0.75-m-wide pedestrian walkways on both sides. It has a total length of 1,680 m spanning the Xijiang River, and it consists of five parts (a total of 43 spans, as shown in Fig. 2): the north approach (13×16 m), north main (7×50 m), main (2×160 m), south main section (13×50 m + 40 m), and south approach (7×16 m) sections. There are expansion (or movement) joints placed between the parts, which are designed to allow for continuous traffic between structures while accommodating movement, shrinkage, and temperature-induced expansion and contraction. The navigation channel lies between Pier No. 20 and Pier No. 22 and is separated by Pier No. 21, which is the pylon of the cable-stayed bridge.

The Vessel Collision Accident

In the early morning of June 15, 2007, a fully loaded 3,000-DWT sand barge diverged from the downstream navigation channel between Pier No. 21 and Pier No. 22 and struck Pier No. 23 of the south main bridge (at a nonnavigation channel). The impact triggered the collapse of a 200-m roadway section along with three piers (Pier Nos. 23–25), resulting in nine fatalities and sinking the barge and four vehicles on the bridge. Fortunately, the progressive collapse stopped at adjacent Pier No. 22 because the end section of the south main bridge (14 span box girders) is fully separated from the girder of the cable-stayed bridge, and thus there should be no load transfer to the latter when the former falls into the water.

Fig. 3 shows a schematic illustration of the damage from the barge collision accident. Fig. 4 shows an enlarged view of the damage near Pier No. 26 and the barge. The cross section of the collapsed span and a vertical view of the collapsed bridge piers (Pier Nos. 23–25) are shown in Figs. 5 and 6, respectively. The pile diameter of the collapsed piers is 1.7 m, and the length is between 43.0 m and 47.8 (Table 1), of which 2 m is embedded into the granite base. The length of the pier columns is approximately 21.1 m, with a hexagonal shape in the cross sections. It was reported that the collision occurred as a result of dense fog conditions on the day of the accident, and the captain was misguided by the light from a nearby construction boat. The water level was approximately at the bottom of the pile caps and was approximately 29.2 m deep at the location of Pier No. 23 when the collision accident happened.

Underwater Detection of the Collapsed Bridge Structures and Colliding Barge

In the effort to understand the underwater distribution and separation of the collapsed spans, a double-frequency sonar system and a multiple-wave-packet depth-measuring system were used to obtain high-definition pictures and ascertain the underwater terrain (He and Zhang 2008). Fig. 7 shows the plan and elevation views of the collapsed parts. Five cuts of the collapsed box girder were observed

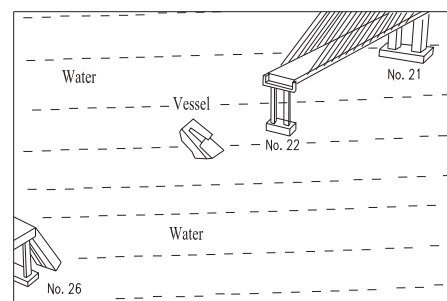


Fig. 3. Bird's-eye view of Jiujiang Bridge shortly after the collision accident

after the collision accident. The first span from Pier 26 is indicated as Cut 1; it was fully separated from the adjacent bridge span and lies on the riverbed. Cut 2 occurred at the end of its adjacent span of 49 m in length and was also fully separated. Three separations (Cuts 3–5) occurred on the span between Pier No. 22 and Pier No. 23, and Cut 4 separated the last collapsed span into two parts (20 and 28 m). The head of the colliding barge went into the riverbed and became covered by the broken box girder between Cut 3 and Cut 4. The condition of the collapsed span between Pier No. 23 and Pier No. 24 remains unknown.

FEA of the Continuous Bridge Subjected to Barge Collision

FE Model—Sand Barge

Table 2 shows the typical dimensions of the type of sand barge involved in the collision, which is sized between the jumbo hopper barge and oversize tank barge used in the U.S. inland waterways (AASHTO 2009). The carrying capacity of this barge is 3,000 tons, and it weighs approximately 3,668 tons with the full-load water discharge. Fig. 8 shows the 3D FE model developed for the barge and the detailed stiffener configuration used for the barge bow. The numerical setup of the barge was carried out according to the construction documentations of the barge, including its general arrangement plan, line plan, transverse cross-sectional plan, and shell-plating expansion line, which were obtained from the barge manufacturer. The FE model of the barge was divided into a head section and the remaining section along its length direction. The head section, with a length of 12 m, was accurately modeled with finer meshes to adequately capture the internal contact between various components, local deformation/buckling, and material failure as best as possible. Various small components in this section, such as small toggle plates, narrow flange plates, and sharp transition plates, were

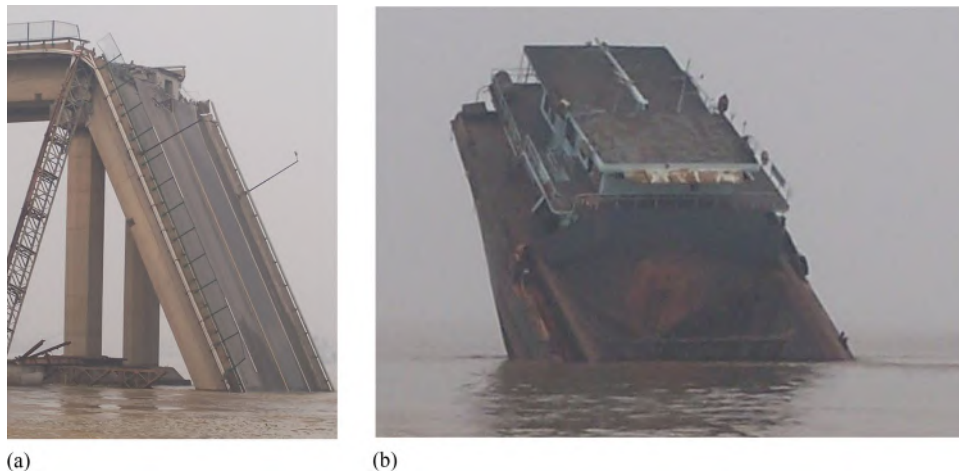


Fig. 4. Photos of the collision accident (images by Hua Jiang): (a) collapsed box girder; (b) colliding vessel

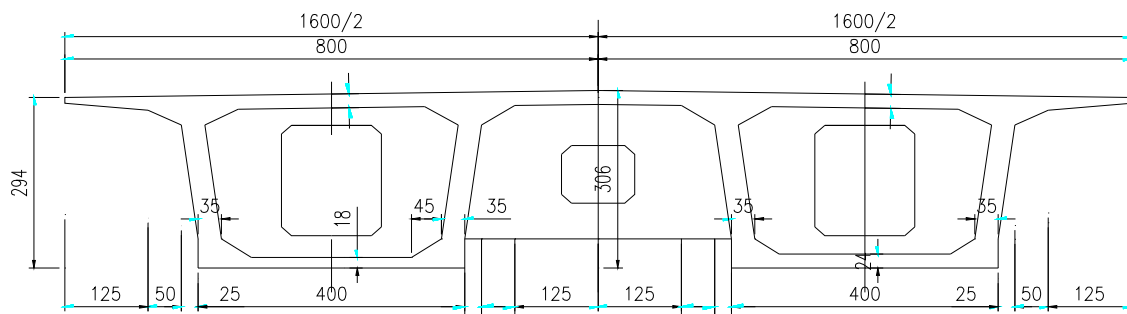


Fig. 5. Cross section of the collapsed bridge girder (unit: cm)

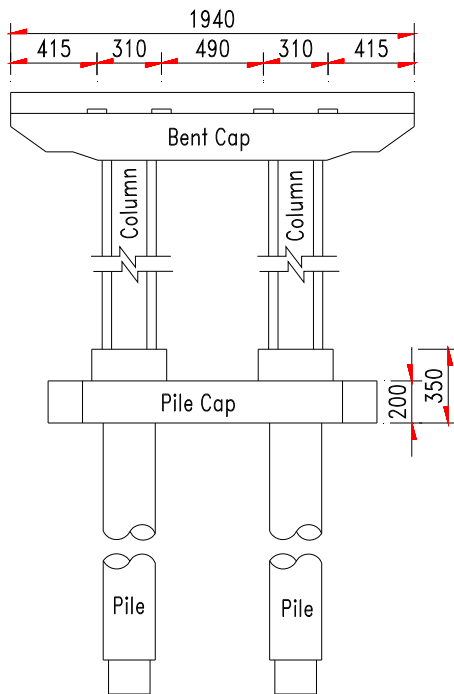


Fig. 6. Vertical view of typical bridge piers (Pier Nos. 23–25) (unit: cm)

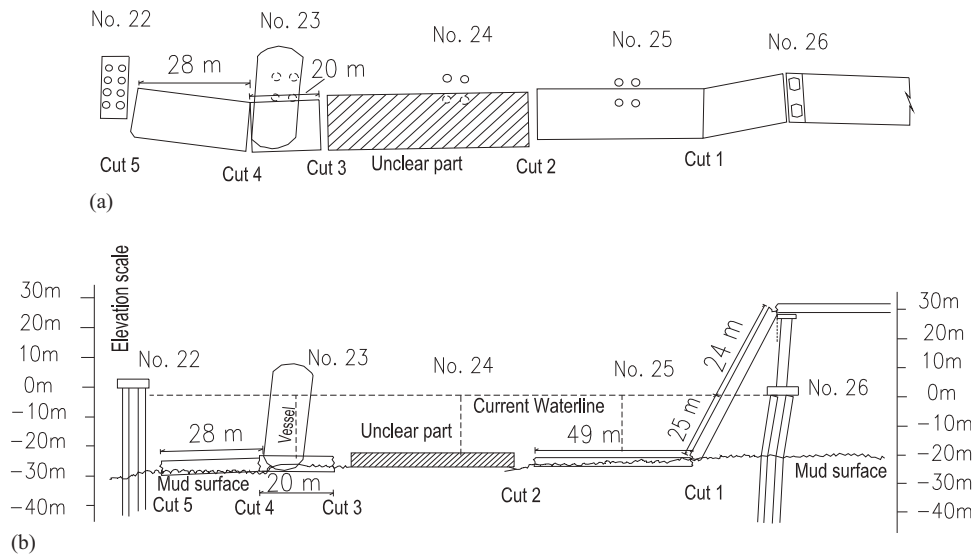
simplified in the model to avoid the use of excessively small elements because the overall time-step size is controlled by the minimum time-step value of each element in the transient analysis, which is further determined by the length of the smallest element. The head section was discretized using four-node shell elements, and the maximum mesh size of the shell elements was 15 cm. The remaining section, with a length of 48 m, was modeled using a relatively coarse mesh, and the minimum mesh size of these elements was 25 cm. The remaining section was modeled as a perfectly rigid element according to the actual shape, mass, and inertial properties because no damage occurred in this region. All of the components in the barge were modeled using the Belytschko–Tsay shell element, with the 1-point Gauss integration scheme and a viscous hourglass control option, which provided high computational efficiency and robustness under severe mesh distortions (Belytschko et al. 2009).

In the numerical simulation, the fully loaded sand barge was considered to be sailing at a velocity of 3.0 m/s according to the in situ measurement of the sailing speed of similar barges after the collision accident. A head-on collision case was considered.

The material model MAT_PLASTIC_KINEMATIC (MAT 3) was employed to represent the mechanical behavior of the barge bow subjected to impact loading. The model features a linear isotropic hardening law and has an option to incorporate the strain-rate effect based on the Cowper and Symonds formulas (Cowper and Symonds 1957). Two parameters, $D = 40.4$, $q = 5$, were selected in the analysis based on the available literature (Jones 1989). Table 3 summarizes other material parameters for the barge bow and the

Table 1. Information on the Collapsed Piers

Pier	Current scouring depth of piles (m)	Maximum designed scouring depth of piles (m)	Total pile length (m)	Pile length above the mud line (m)	Embedded length in rock (m)
23	15.8	23.8	47.8	30.2	2
24	15.5	17.6	33.3	29.7	2
25	3.5	6.8	35.0	29.2	2

**Fig. 7.** Underwater detection of the collapsed bridge structures after the collision: (a) plan view; (b) elevation view**Table 2.** Typical Characteristics of the Barge Type Involved in the Accident

Symbol	Barge involved in the accident	Jumbo hopper	Oversize tank
L_B = length (m)	75.18	59.44	88.39
B_M = width (m)	15.35	10.67	16.15
H_L = head log height (m)	—	0.61–0.91	0.61–0.91
R_L = bow rake length (m)	—	6.10	7.62
D_v = depth of vessel (m)	4.5	3.7	3.7
D_E = empty draft (m)	0.94	0.5	0.5
D_L = loaded draft (m)	2.6	2.7	2.7
C_c = cargo capacity (tons)	3,000	1,700	3,700
W_E = empty displacement (tons)	668	200	600
W_L = loaded displacement (tons)	3,668	1,900	4,300

reinforcement, where Reinforcement 1 denotes the transverse reinforcement in structural members (e.g., pier column, piles, and box girder), and Reinforcement 2 denotes the longitudinal reinforcement with high yield strength used in structural members.

FE—Prestressed Concrete Bridge

Because the collision occurred at Pier No. 23 of the south main bridge with two expansion joints at the end of the bridge deck (Fig. 2), only the south main bridge was modeled in *LS-DYNA*. This section has a 14-span continuous PC box girder (690 m long and 16,720 tonnage) and 15 piers (Pier Nos. 22–36), as shown Fig. 2. Detailed design information for the steel reinforcement and prestressed tendons in the structural members is provided in Table 4.

As shown in Fig. 9, two single-cell boxes with uniform height were created side by side to make up a superstructure, and each RC

pier in the simulation was composed of two pier columns, one bent cap, four piles, and their pile caps. Both the box girder and piers above the scour line were discretized with 8-node constant-stress solid elements, and a fine mesh with a minimum mesh size of 1 cm was adopted in the collision area of the pier column, whereas a coarse mesh size of 50 cm was used for the box girder. The surface between the fine mesh and coarse mesh elements was rigidly constrained. Piles below the scour line were modeled using the Belytschko–Schwer beam elements, in which nonlinear P–Y springs were applied along the length of beams at an interval of 1.5 m to model the lateral soil–pile interaction. The P–Y curves for different types of sand (including fine sand, medium sand, and coarse sand) were obtained using the nonlinear FEA program *FB-MultiPier*. For example, the required input parameters used to generate P–Y curves for cohesionless soil include the internal friction angle (ψ), total unit weight (γ), subgrade modulus K , and diameter of the pile (D). Table 5 demonstrates the soil properties at the position of Pier No. 23; the underlying soil consists of coarse sand, gravelly sand, and microweathered granite, respectively.

The pile base was modeled using a fixed boundary condition because the bridge piles are embedded into the bedrock beneath the sand layers. The interface between the top end of the beam elements and the bottom surface of the solid elements was modeled by assigning a nodal rigid-body constraint. To model the progressive collapse of the bridge structure and characterize the structural damage in the riverbed, the riverbed surface was created using shell elements. In this study, an elastic constitutive model was used for the riverbed surface soil because P–Y springs have been successfully applied to model the interaction effects between pile and soil (McVay et al. 2009). The modulus of elasticity for loose sand and medium dense sand was assumed to be 15.0 and 17.25 MPa, respectively (FHWA 2004).

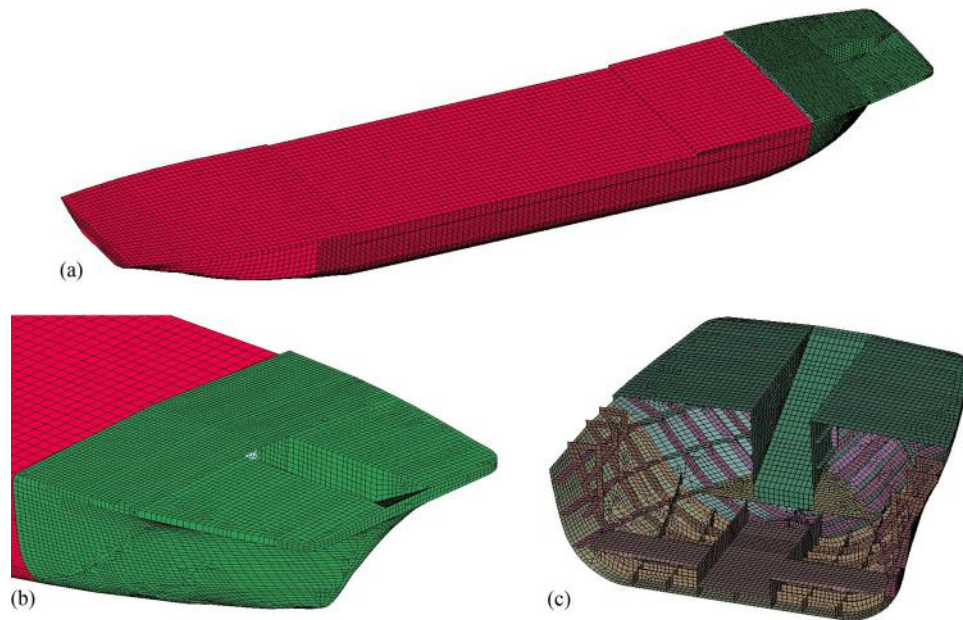


Fig. 8. FE model developed for the sand barge: (a) 3D view; (b) enlarged view—barge head; (c) enlarged view—barge-head details

Table 3. Material Parameters for Barge Bow and Reinforcement

Type	Density ρ (kg/m ³)	Elasticity modulus E (GPa)	Tangent modulus E_T (GPa)	Poisson's ratio ν	Yield stress σ (MPa)	Erosion strain
Barge bow	7,850	200	1.5	0.3	235	0.35
Reinforcement 1	7,850	200	1.2	0.3	235	0.35
Reinforcement 2	7,850	210	1.2	0.3	340	0.35

Table 4. Design Information of the Steel Reinforcements and Prestressed Tendons for Bridge Piers and Superstructure

Bridge member	Structural type	Longitudinal reinforcement		Transverse reinforcement		Longitudinal prestressed tendon	
		D (mm)	Number	D (mm)	Interval (mm)	S (mm ²) $\times N$	Number
Pier column	RC	22	42	8	250	—	—
Pile	RC	22	24	8	200	—	—
Girder	PC	16	180	8	150	140 \times 9	16

The Continuous Surface Cap Model (MAT 145) available in *LS-DYNA* was used in the simulation of the typical concrete material response for impact loading. It is an elastoplastic damage model and well captures important mechanistic behaviors of concrete under complex static and dynamic loading conditions. The model has been calibrated for a wide range of concrete (C10–C70), and the material parameters can be determined based on the uniaxial compressive strength of concrete and the maximum aggregate size (Jiang and Zhao 2015). It has also been validated for RC beams subject to a falling-weight impact (Jiang et al. 2012a). The subsequent simulation adopted the Young's modulus of 28.5 GPa for concrete substructures where Chinese Grade C23 concrete was used and a value of 35.0 GPa for the box girders, which were constructed with Chinese Grade C50 concrete per JTG D62-2004 (Ministry of Transport of the P.R.C. 2004). The parameters of the MAT 145 model adopted in the study are summarized in Table 6. Constant-stress 8-node solid elements with a 1-point quadrature integration scheme were used to model the structural concrete. In the simulation, solid elements were automatically removed from the numerical simulation when the damage (including both ductile damage

and brittle damage) in the elements reached 1, which represents the fully damaged state of a concrete element.

The steel reinforcement in concrete [Figs. 9(c and e)], including the prestressing tendons, was modeled using Hughes–Liu beam elements with a 2×2 Gauss cross-sectional integration, which has high computational efficiency and robustness (LSTC 2015). The prestressing force in concrete was applied by imposing a temperature-induced shrinkage in prestressing stands, as described in detail in the validation section.

Simulation of the Barge Colliding with the Bridge

To simulate the contact behavior between the barge bow and pier column, a surface-to-surface constraint algorithm with friction was used, in which the static and dynamic friction coefficients of 0.5 and 0.3 (Consolazio et al. 2009), respectively, were used to consider the friction between steel and concrete. This approach was used to simulate the friction forces transmitted across the contact interface. The initial distance between the barge bow and pier column was set to be 10 mm to save computational time and to avoid an initial

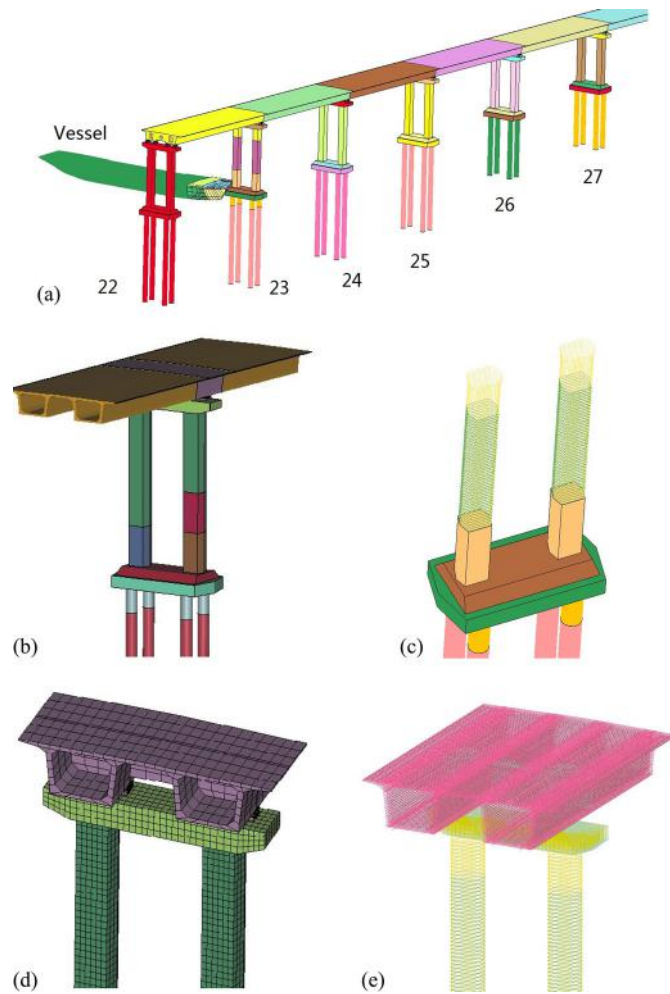


Fig. 9. FE model developed for bridge piers and superstructure: (a) multiplier models; (b) Pier No. 23 and associated superstructure; (c) meshing rebar elements in pier columns; (d) enlarged view of Pier No. 23 and associated superstructure; (e) meshing rebar elements in superstructure

Table 5. Properties of Soil under Pier No. 23

Soil type	Thickness (m)	Total unit weight γ (kN·m ⁻³)	Internal friction angle φ (degree)	Subgrade modulus K (kN·m ⁻³)	Standard penetration test N_{SPT}
Coarse sand	18.2	19	35	26,000	30
Gravelly sand	4.4	21	38	40,000	38

Note: Microweathered granite under the gravelly sand is not included in the table.

penetration between the surface of the shells (barge bow) and solid elements (pier column) during a transient analysis. In addition, the contact between the barge bow and the bridge pier was carefully defined, and the self-contact in the barge bow was also considered to detect any self-contact of its components resulting from significant deformation throughout the collision analysis.

To simulate the progressive collapse of the bridge structure and the sinking mechanism of the barge, a surface-to-surface contact was defined among the box girders, piers, barge, and riverbed surface. Two groups, namely, the barge group and the bridge pier group, were defined. The former was composed of the barge-bow section and the remaining section, and the latter was composed of the bent cap, pier columns, pile cap, and piles. Table 7 summarizes the main contact groups used in the numerical simulation. Acceleration resulting from gravity (or the weight of the barge and bridge structure) was taken into account to model the phenomenon

of the separating and sinking of any broken bridge components and the sinking of a portion of the barge during the collision. The keyword *LOAD_BODY cards of *LS-DYNA* were used.

To better characterize the interaction behavior of the box girder and the bridge pier through bridge bearings, a simplified FE model for the bridge pot rubber bearings including two-way movable pot-type bearings, one-way movable pot-type bearings, and fixed pot-type bearings was set up and is shown in Fig. 10. The connections between the sole plate of the bridge bearing and the bottom surface of the PC girder and the masonry plate of the bridge bearing and the bent cap of the pier were also rigidly constrained. The interaction behavior between the sole plate and masonry plate in the preload stage and in the vessel-bridge collision stage was modeled by *CONTACT_AUTOMATIC_SURFACE_TO_SURFACE_MORTAR and *CONTACT_AUTOMATIC_SURFACE_TO_SURFACE, respectively.

Drop-Weight Impact Tests for Validation of Barge–Bridge Collision Model

The FE model of the multispan continuous bridge subjected to a barge collision was validated by comparing the numerical response and test results of drop-weight impact tests on RC and PC beams. The impact tests of a RC beam and a PC beam were conducted by Fujikake et al. (2009) and Kelly (2011), respectively. The purpose of this step was to validate the performance of two major components in the FEA model: (1) RC components, such as pier columns and piles, subjected to impact loading; and (2) PC components, such as bridge girders, subjected to impact

Table 6. Parameters of the Continuous Surface Cap Model for Concrete Grades C23, C47, and C50

Concrete grade	C23	C47	C50
α (MPa)	5.6298	13.7647	14.9516
θ	0.3437	0.3293	0.3272
λ (MPa)	1.8112	7.1831	8.1299
β (MPa ⁻¹)	0.0837	0.0245	0.0240
α_1 (MPa)	0.82	0.82	0.82
θ_1	0.0	0.0	0.0
λ_1 (MPa)	0.2407	0.2407	0.2407
β_1 (MPa ⁻¹)	0.016867	0.008531	0.008317
α_2 (MPa)	0.76	0.76	0.76
θ_2	0.0	0.0	0.0
λ_2 (MPa)	0.25616	0.25616	0.25616
β_2 (MPa ⁻¹)	0.014566	0.007396	0.0071
X_0 (MPa)	60.603	106.011	108.14
D_1 (MPa ⁻¹)	6.11×10^{-4}	6.11×10^{-4}	6.11×10^{-4}
D_2 (MPa ⁻²)	2.225×10^{-6}	2.225×10^{-6}	2.225×10^{-6}
W	0.065	0.065	0.065
S	1.977	1.955	2.0
A^-	1.0	1.0	1.0
B^-	0.1	0.1	0.1
A^+	1.0	1.0	1.0
B^+	0.3	0.2	0.3

Note: Units = mm, ton, sec, N.

Table 7. Contact Used in the Course of Barge–Bridge Collision

Type	Barge	Box girder	Bridge pier	Riverbed
Barge	1	2	2	2
Box girder	—	2	2	2
Bridge pier	—	—	2	2

Note: 1 = automatic single-surface contact; 2 = automatic surface-to-surface contact.

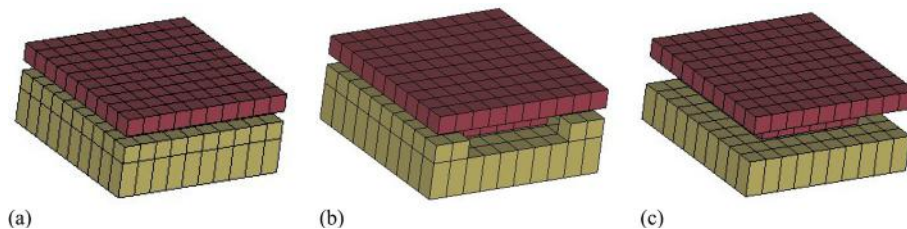


Fig. 10. Simplified FE model developed for the pot-type elastomeric pad bearings: (a) fixed pot-type bearing; (b) one-way movable pot-type bearing; (c) two-way movable pot-type bearing

loading. The validation of the FE model using the impact test of a RC beam is not shown here because a detailed introduction can be found in previous papers (Jiang et al. 2012b; Jiang and Zhao 2015).

An impact test involving a PC beam was reported by Kelly (2011). The PC beam was simply supported and had a span of 3,000 mm, and its cross-sectional dimension was 250×150 mm. The uniaxial compression strength of the concrete was 47 MPa. Two steel strands with a 150-mm^2 cross-sectional area and steel grade of 1,860 MPa were used, with an eccentricity of 32.5 mm below the neutral axis. The applied prestressing force was 390 kN. The longitudinal reinforcement in both the tension and compression sides consisted of two 6-mm-diameter mild steel bars with 25-mm concrete cover. The stirrups (with a diameter of 6 mm) were spaced at 200-mm intervals. A solid steel impactor with a mass of 221.4 kg was dropped freely from the height of 1.25 m to directly strike the top face of the beam at the position of midspan. The recorded impact force and midspan displacement were considered for this validation.

In the FE model, the newly calibrated elastoplastic damage model MAT 145 was used for the concrete and MAT-RIGID (MAT 20) was used for the impactor. The steel reinforcements were meshed using truss elements with a mesh size of 25 mm. In the collision simulation, the prestressing force was applied to the concrete member by imposing a temperature-induced shrinkage in the prestressing stands. Therefore, a drop of 619°C (reference temperature 0°C) and $\alpha = 1 \times 10^{-5}/^\circ\text{C}$ in the strands can produce an equivalent force in this PC beam (Jiang and Chorzepa 2015b). This stress initialization process was completed prior to performing a transient analysis by the dynamic relaxation method with a control card *CONTROL_DYNAMIC_RELAXATION (LSTC 2010) in LS-DYNA. Both PC beam and impactor were represented by hexahedron elements with one integration point and maximum mesh size of 10 mm.

Fig. 11 compares the time histories for impact force and midspan displacement. The two large clear peaks found in the impact force–time histories from the experiment and numerical simulations were very similar. The impact force after 4 ms obtained from the numerical simulation differed from the force–time relationship observed in the experiment because some eroded elements had been fully removed while still in contact with the impactor. The predicted midspan displacement generally agreed with the numerical results, particularly before 40 ms, but the residual displacement was a little larger than the experimental results. Fig. 12 shows a comparison of the damage pattern of the PC beam after the drop-weight impact. The spalling and cracks in the PC beam observed in the test were generally well captured in the numerical results by eroding the fully damaged elements. Therefore, the MAT 145 model used in this analysis appears sufficient to represent concrete damage in the impact zone.

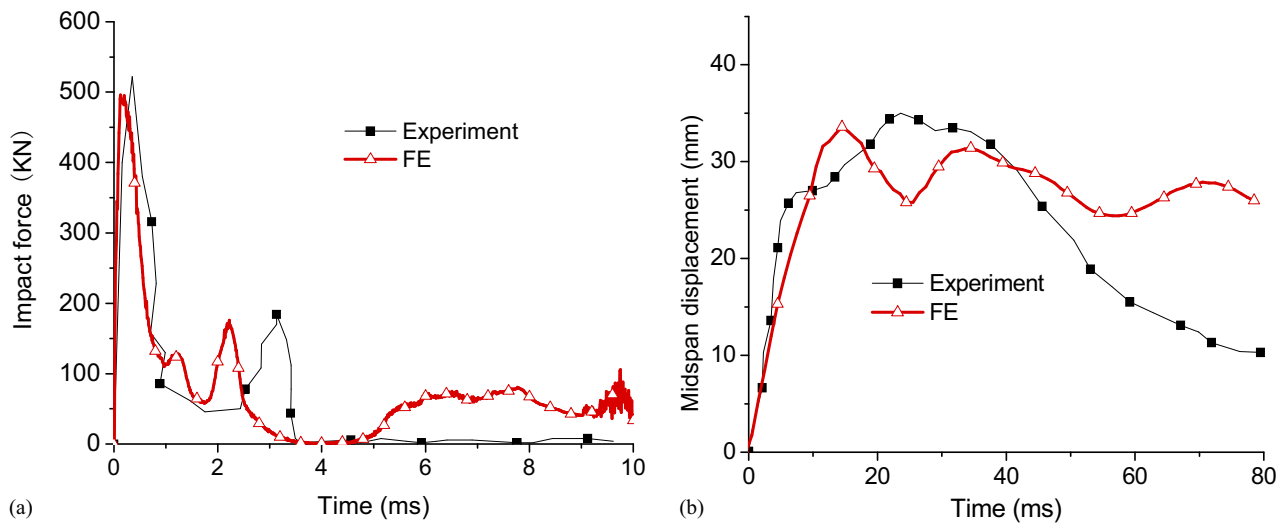


Fig. 11. Comparison of results: (a) impact force; (b) midspan displacement

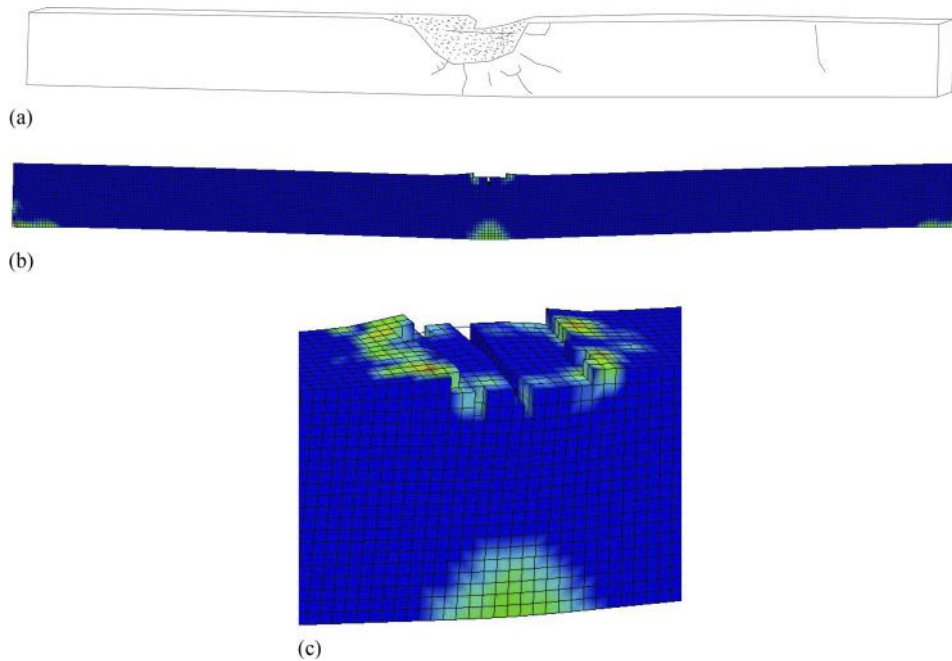


Fig. 12. Comparison of damage pattern: (a) test specimen showing the location of spalling and cracks in concrete; (b) numerical results showing location of eroded elements and damage contours; (c) enlarged view of the local damage

Simulation Results of the Progressive Collapse of a Multispan Continuous Bridge

Progression of the Bridge Failure and Failure Mechanism

Figs. 13(a–j) illustrate the simulated progressive collapse of three bridge piers, four spans of the superstructure, and the sinking mechanism of the colliding barge as the barge collided into Pier No. 23. The simulation results indicate the following failure mechanism:

1. The barge collided into Pier No. 23, resulting in the lateral displacement of a pile cap and substantial damage in the pier columns and supporting piles [Fig. 13(b)].

2. The lateral displacement of the pile cap led to the downward vertical displacement of the bent cap, which caused a separation of the bearings under the box girder.
3. Because of the large vertical displacement of the continuous span at the junction of Pier No. 23, the left end section of the span began to slide off of Pier No. 22, followed by a breakup of the box girder at the junction of Pier No. 24 [Fig. 13(c)].
4. While Pier No. 23 started to collapse with the large lateral and vertical displacements, the continuous span of the superstructure between Pier No. 22 and Pier No. 24 began to deflect at the midspan (or Pier 23 location) as a result of the girder self-weight, and it struck the barge head, sinking a portion of the barge as a result of the eccentric load.

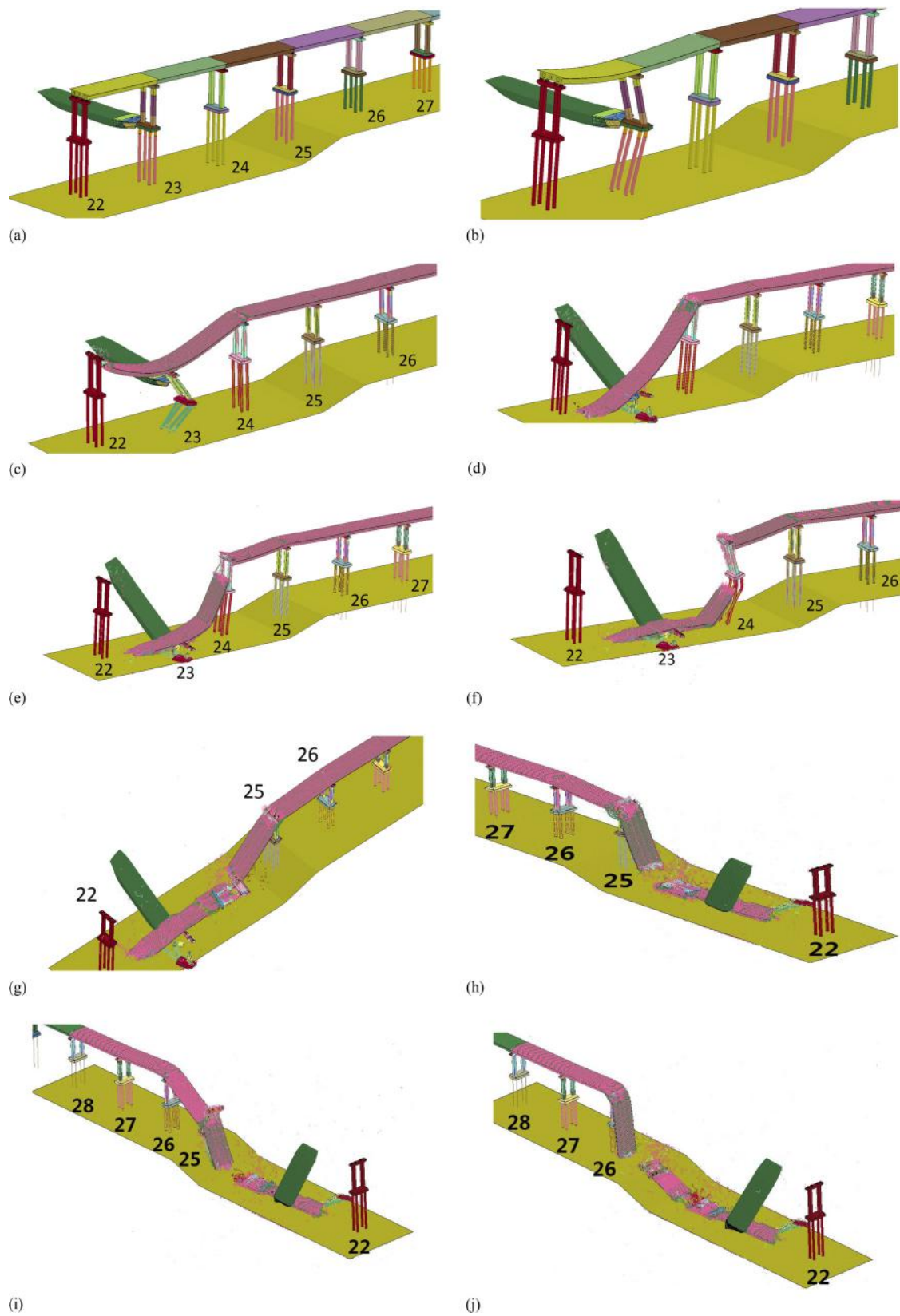


Fig. 13. Simulated progressive collapse of the continuous bridge subject to a barge collision: (a) 0.0 s; (b) 5.0 s; (c) 8.0 s; (d) 11.0 s; (e) 13.0 s; (f) 15.0 s; (g) 18.5 s; (h) 20.0 s; (i) 23.0 s; (j) 25.0 s

5. Finally, the collapsed span also displaced the adjacent span connected to Pier No. 24 and Pier No. 25 [Fig. 13(d)] because the collapsed girder was connected to its neighboring girder by the continuous tendons and longitudinal reinforcements.

The right end portion of the collapsed superstructure struck Pier No. 24 as it fell [Fig. 13(e)] and eventually caused the collapse of this pier by large longitudinal thrust [Fig. 13(f)]. When Pier No. 24 began to collapse, the box girder above began to rotate clockwise around the section at the junction of Pier No. 25 as a result of gravity and soon broke the girder at the junction of Pier No. 25 [Fig. 13(g)]. The new broken end fell down, collided with Pier No. 25, and pushed over this pier by large thrust [Fig. 13(i)].

Similar to the collapse process of the adjacent span, the box girder connecting Pier No. 25 and Pier No. 26 began to rotate clockwise around the section at the junction of Pier No. 26 as a result of gravity, and breaks at the junction of Pier No. 26 appeared [Fig. 13(i)]. The span connecting Pier No. 25 and Pier No. 26 then rested between the riverbed surface and Pier 26 [Fig. 13(j)]. The progressive collapse stopped at this span because the end section corresponding to the Pier No. 25 location came into contact with the riverbed surface, which prevented this span from dropping into the river and reduced the magnitude of the lateral thrust against Pier No. 26. It was determined that the elevation of the riverbed surface at the support position was approximately 10 m higher than that

measured at the other locations (e.g., Pier Nos. 22–25), which offered favorable terrain conditions to support the end section (Cut 1). Otherwise, the inclined span running between Pier 26 and the riverbed may have been completely submerged in the river, and the progressive collapse might have extended beyond Pier 26.

It was also determined from the simulation that the submerged portion of the barge and warped barge stern were caused by the collision between the box girders and barge bow. This agrees well with the real case [Figs. 4(b) and 7]. The number of collapsed piers and spans obtained from the numerical results and in documented accident reports are identical. In both cases (numerical simulation and collision accident), Pier No. 22 did not collapse (Fig. 13) because of a separation of the continuous spans of the south main bridge from the spans of the main bridge by an expansion joint. It is noteworthy that the damaged superstructure obtained from the numerical simulation [Fig. 13(j)] exhibited some similarities with the damage phenomenon obtained from underwater detection (Fig. 7). The discrepancy could be attributable to the limited treatment of soil modeling (e.g., P-Y spring and elastic riverbed surface) because the collision of the barge and bridge structural members could lead to large plastic deformation and damage behavior of the soil in the riverbed.

Figs. 14(a–f) present a schematic summary of the progressive collapse mechanism involving the multispan continuous bridge in an elevation view. It is shown that the collapse of Pier No. 23 was

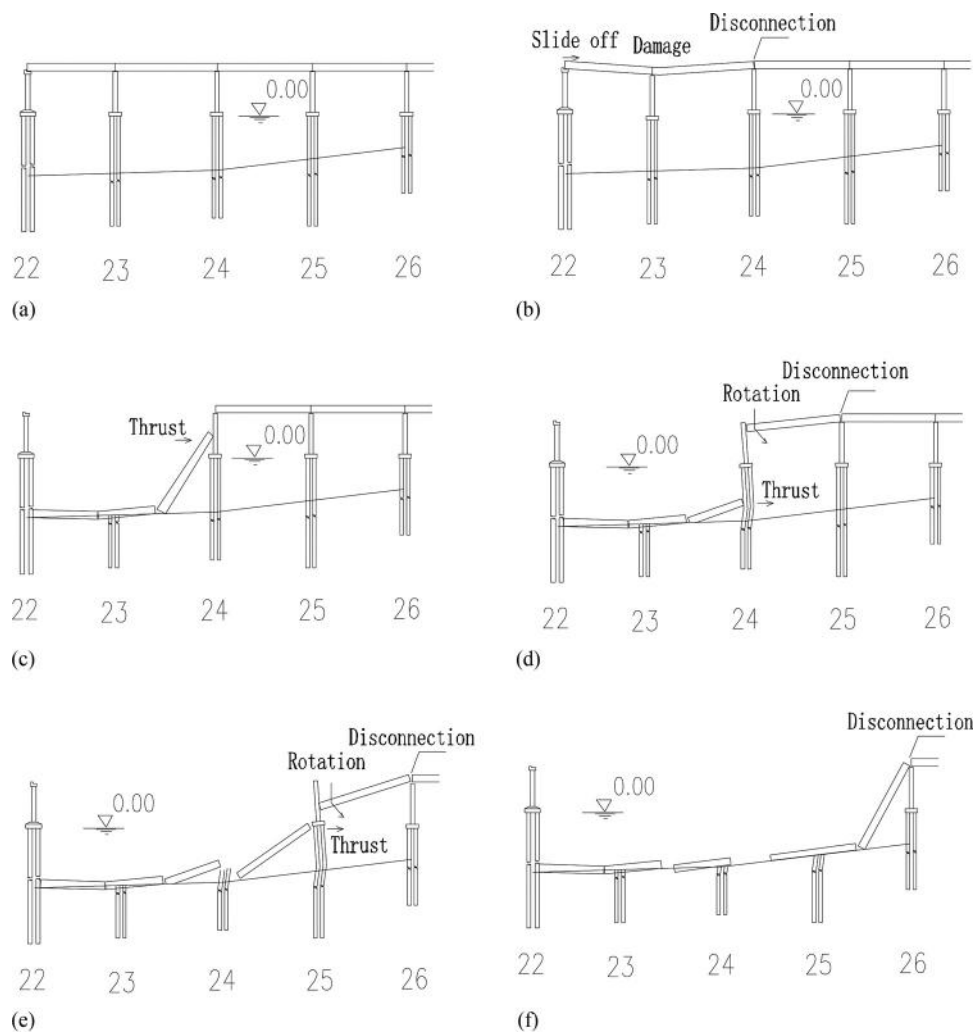


Fig. 14. Summary of the collapse progression

directly caused by lateral barge collision, whereas the failure of Pier No. 24 and Pier No. 25 was caused by the falling-weight impact of a collapsed span in the longitudinal direction.

Collapse Mechanism of Impacted Pier (Pier No. 23)

Fig. 15 illustrates the collapse mechanism of Pier No. 23 by providing a cross-sectional elevation view at the pier location. The displacement at the pile cap was greater than the displacement at the bent cap [Fig. 15(c)] because the pile cap region received a direct impact from the barge, whereas the movement of the bent cap was constrained by the bridge superstructure. In this study, the movement of the pile base was also constrained by soil resistance at the riverbed. The pier column first failed at the collision location of the impacted pier column and at the base of the adjacent pier column (at approximately 2.0 s), where a large amount of concrete elements were eroded in the simulation model. Subsequently, the top region of the impacted pier column and the adjacent pier column started to fail (at approximately 5.0 s). The successive failing parts were at the top and bottom portions of the pile [Fig. 15(d)]. In the course of the barge collision, both the pier columns and piles appeared to show large lateral displacements before they collapsed. There were observed plastic-hinge bending deformations in the piles and pier

columns. For example, the maximum length of the plastic hinges near the top end of the piles and pier column is approximately 1.5 and 1.0 m, respectively. Hence, the failure of the slender piles (a length of 30.2 m above the riverbed surface) and pier columns (a length of 21.2 m) can be regarded as plastic-hinge bending failure. It is also important to note that the failure mode of the piles near the riverbed surface may have been overestimated because a rigid-plane boundary was used to connect the bottom section of the solid elements as well as the top section of the beam elements in the numerical model, making the section near the riverbed surface rigid. It is also clearly shown in this figure that the downward displacement of the impacted pier resulted in a separation of the girder from the upper bearing components, such that the vertical supports for the girders were suddenly lost, which resulted in crack formation and damage in the girder. The collapse process was exacerbated by gravity because of the weight of the bridge superstructure.

Further Investigation on the Collision Response of Impacted and Adjacent Piers (Pier No. 23 and Pier No. 24)

From the numerical study just presented, it is evident that the collapse of Pier No. 23 (impacted pier) led to the progressive collapse

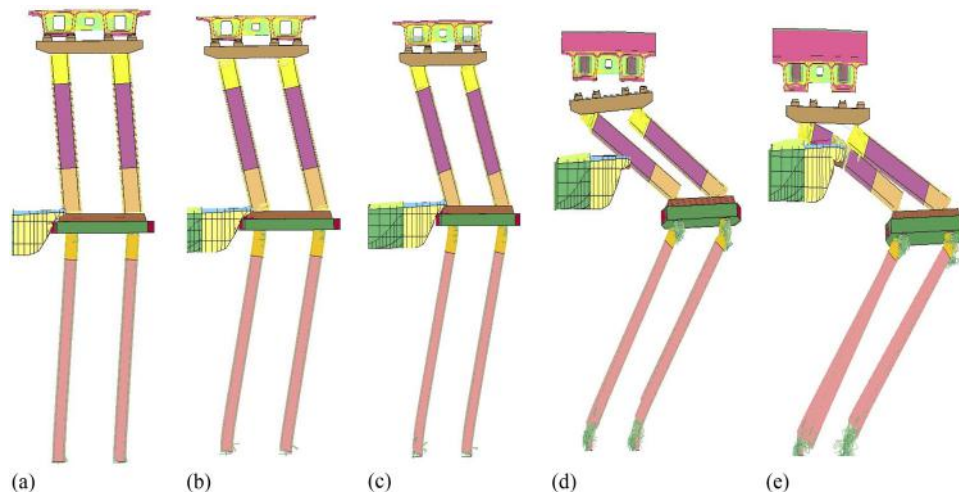


Fig. 15. Schematics showing the progression of Pier No. 23 collapse: (a) 1.5 s; (b) 4.0 s; (c) 5.0 s; (d) 7.5 s; (e) 8.0 s

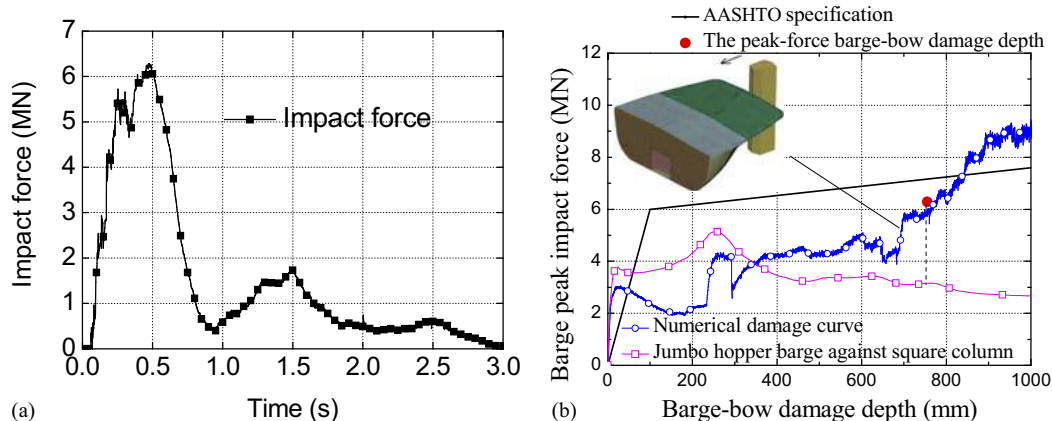


Fig. 16. Impact force that acted on Pier No. 23: (a) force-time history; (b) comparison of the peak-value barge-bow damage depth with AASHTO specifications and numerical damage curves

of other parts of the continuous bridge. It is critically important to investigate the collision response of this particular pier in detail.

Fig. 16(a) presents the impact force determined from the vessel–bridge collision simulation. The peak impact force was 6.3 MN, and the corresponding barge-bow crush depth was 0.754 m. The static barge-bow force–deformation relationship (referred to as the crush-depth curve hereafter) is provided in Fig. 16(b), where the rigid pier column (having the same shape and size as the pier column in Pier No. 23) was forced into the barge-bow model with a fixed rear section at a prescribed velocity of 125 mm/s. The peak impact force shown in Fig. 16(a) [a circular point in Fig. 16(b)] was larger than the value obtained from the barge-bow crush–depth curve. The barge-bow crush–depth curve for a jumbo hopper barge against a

push from a square pier (Consolazio and Cowan 2005) is presented in Fig. 16(a). The relationship between peak impact force and barge crush depth determined by the AASHTO specifications for U.S. inland barges (AASHTO 2009) is also shown. The peak force that resulted from the sand barge was lower than the corresponding value provided in the AASHTO specifications. The barge-bow crush–depth curve of the sand barge significantly differed from that of the jumbo hopper barge because of the structural difference in the barge bow and geometric differences, such as in pier column shape and size. In addition, the static lateral bearing capacity of Pier No. 23 was obtained from a pushover analysis using *FB-MultiPier*. The estimated maximum static lateral load applied at the position of the collision area was approximately 1.30 MN (Wang and Jiang

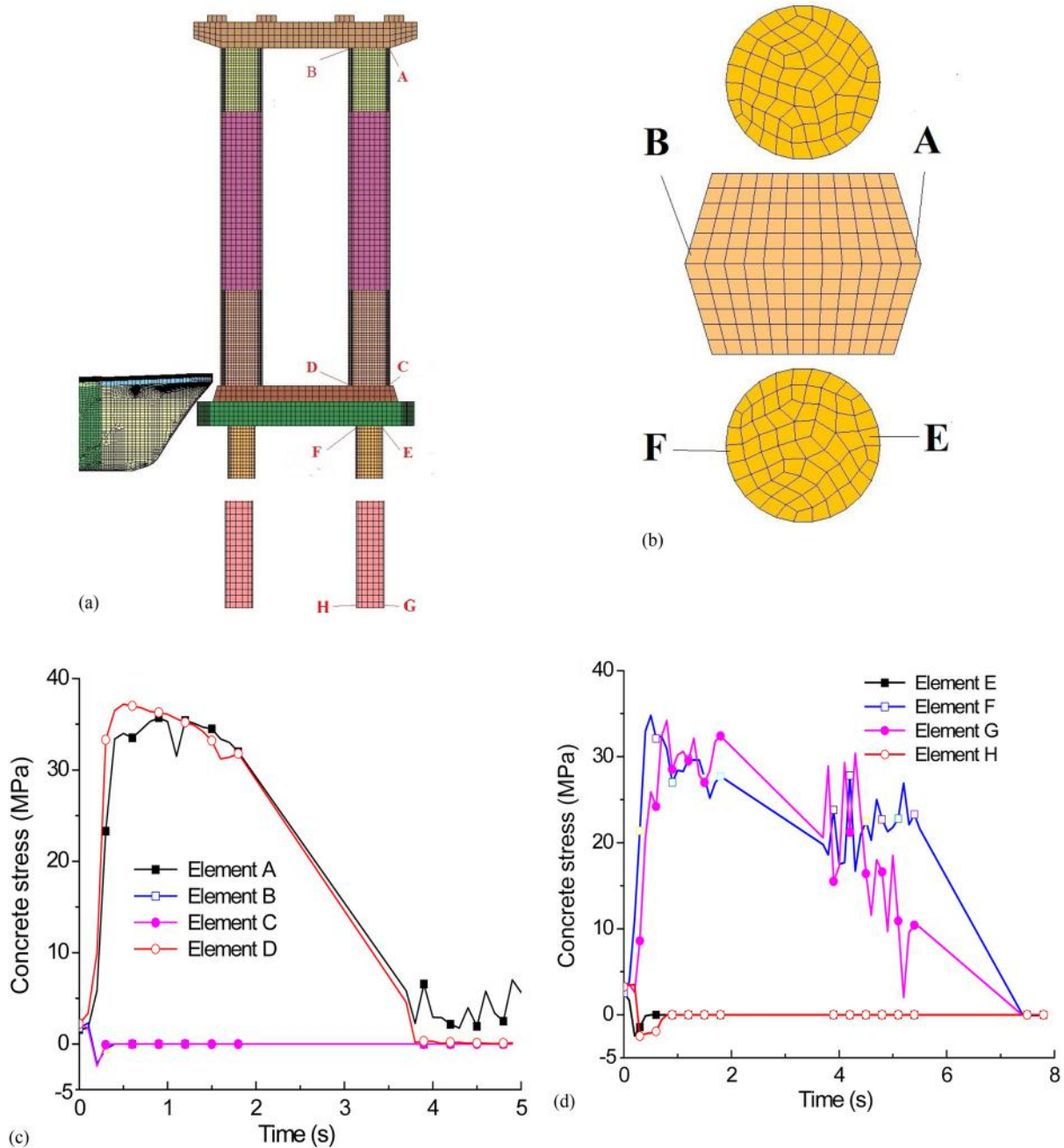


Fig. 17. Stress plots of concrete elements in Pier No. 23: (a) at the position of adjacent pier column and piles; (b) cross sections of column and piles with studied elements; (c) stress on pier column; (d) stress on piles

2011), which is much smaller than the peak value of the dynamic force. Therefore, it is reasonable that Pier No. 23 would fail under such a large impact load.

Fig. 17 shows the concrete stress in the extreme fiber of the top and bottom concrete sections of the pier column and piles during the barge collision, where the compressive stress is considered positive. Relatively large compressive stresses were observed at Positions A and D for the pier column and at Positions F and G for the piles, whereas the compressive stress on the opposite edge was very small (less than 3 MPa) for both the pier column and piles. The peak stress on Elements A, D, and F was larger than the uniaxial compressive strength for C23 concrete because the MAT 145 model can automatically consider the strength increase from including strain-rate and confinement effects for concrete. It was also found that the stresses on Elements B, D, E, and G reversed from compression to tension, and the tension stress dropped from the maximum value to zero and remained at zero, which corresponded to the state of fully damaged concrete elements. Consequently, the column/pile sections were subjected to eccentric compression loading.

Fig. 18(a) demonstrates the distribution of the bending moments at the position of the two ends of the pier columns and piles resulting from the barge collision. These moment forces were estimated from a cross-sectional stress analysis of concrete. The direction of the bending moment was obtained from the simple model shown in Fig. 18(b), where the pile cap was imposed a lateral displacement with a fixed boundary condition at the top of the bent cap and at the bottom of the pile. This assumption on the boundary condition was derived from the observation of the lateral displacement of Pier No. 23 shown in Fig. 15.

Fig. 19 includes a plot of the force that acted on Pier No. 24, which was caused by a collision of the destructed spans. The peak value (12.5 MN) in the longitudinal direction of the bridge was almost twice as large as the peak impact force (6.3 MN) that acted laterally on Pier No. 23 [Fig. 16(a)]. The large vertical force on this

pier exacerbated the failure of the pier. In general, the longitudinal resistance of a pier is expected to be smaller than its lateral resistance. Hence, the collapse of Pier No. 24 in the longitudinal direction is inevitable when a collapse of Pier No. 23 in the lateral direction has occurred. In a similar manner, Pier No. 25 collapsed in the longitudinal direction of the bridge.

Conclusions

This paper described a numerical study of the progressive collapse of multiple piers and spans of a 14-span continuous bridge resulting from vessel collision using *LS-DYNA*. The analysis results were found to agree well with the observed failure phenomena of a bridge collapse resulting from vessel collision. The major conclusions drawn from this study can be summarized as follows:

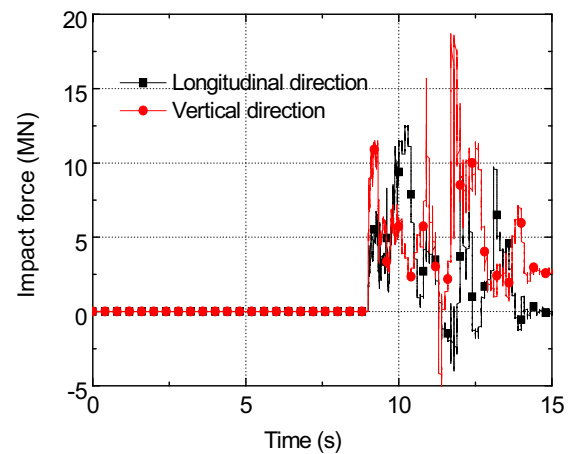


Fig. 19. Impact force that acted on Pier No. 24

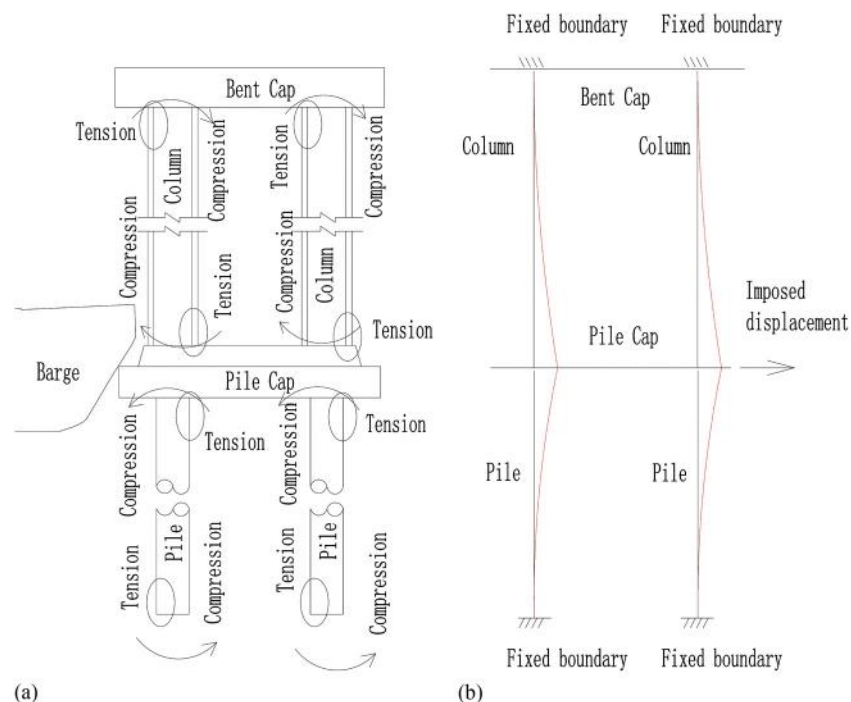


Fig. 18. Illustration of barge collision-induced bending moments in Pier No. 23: (a) at the position of two ends of pier columns and piles; (b) a simplified model for barge impact

1. The progressive failure of the multispan continuous bridge includes a collapse of several bridge piers and spans. The bridge pier directly impacted by a vessel collision fails in the lateral direction of the bridge span as a result of large lateral vessel collision loads, whereas other piers collapse in the longitudinal direction of the bridge span. The collapses of non-impacted piers are caused by the forces generated from the destructed spans during the progressive failure of the superstructure.
2. The number of the collapsed spans and piers depends on underwater terrain conditions. The progressive collapse may discontinue when the end section of the subsiding span comes into contact with the riverbed surface in the shallow water. The failure of the pier columns and piles results from plastic bending of the slender structural members.
3. The peak barge impact force applied to the impacted pier was a little larger than the value predicted by the barge-bow force-deformation curve determined from the numerical analysis but is smaller than that predicted by the AASHTO specifications. The submergence of the colliding vessel was not caused by the impact force between the vessel and bridge pier but resulted from the impact of fragmented pieces of bridge superstructures.

Acknowledgments

The first and second authors are grateful for the financial support from the National Science Foundation of China (Grants 51308054, 51278373, and 51438010) and the DOT of China under the contracts 2007-318-822-34 and 2008-353-344-340. We are grateful to Mr. Pan Fang, Wu Yucai, and Zhang Hailong of the Guangdong Expressway Company for providing design information for the collapsed bridge and sinking barge, which made this study possible. We also thank Mr. Zhao Kai (a MS graduate from Tongji Univ.) for setting up the FE model of the prestressing stands. The opinions, findings, and conclusions do not reflect the views of the funding institutions, bridge owners, or other individuals.

References

- AASHTO. (2009). *Guide specification and commentary for vessel collision design of highway bridges*, 2nd Ed., Washington, DC.
- ADINA [Computer software]. Adina R&D, Watertown, MA.
- Belytschko, T., Liu, W. K., and Moran, B. (2009). *Nonlinear finite elements for continua and structures*, Wiley, New York.
- BSI (Bridge Software Institute). (2010). *FB-MultiPier user's manual*, Univ. of Florida, Gainesville, FL.
- Chu, L. M., and Zhang, L. M. (2011). "Centrifuge modeling of ship impact loads on bridge pile foundations." *J. Geotech. Geoenviron. Eng.*, **10.1061/(ASCE)GT.1943-5606.0000446**, 405–420.
- Consolazio, G. R., Cook, R. A., Lehr, G. B., Bollmann, H. T. (2002). "Barge impacting test of the St. George Island causeway bridge. Phase I: Feasibility study." *Structures Research Rep. No. 783*, Engineering and Industrial Experiment Station, Univ. of Florida, Gainesville, FL.
- Consolazio, G. R., and Cowan, D. R. (2003). "Nonlinear analysis of barge crush behavior and its relationship to impact resistant bridge design." *Comput. Struct.*, **81**(8–11), 547–557.
- Consolazio, G. R., and Cowan, D. R. (2005). "Numerically efficient dynamic analysis of barge collisions with bridge piers." *J. Struct. Eng.*, **10.1061/(ASCE)0733-9445(2005)131:8(1256)**, 1256–1266.
- Consolazio, G. R., Cowan, D. R., Biggs, A., Cook, R. A., Ansley, M., Bollmann, H. T. (2005). "Full-scale experimental measurement of barge impact loads on bridge piers." *Transp. Res. Rec.*, 1936, 81–93.
- Consolazio, G. R., and Davidson, M. T. (2008). "Simplified dynamic analysis of barge collision for bridge design." *Transp. Res. Rec.*, **2050**, 13–25.
- Consolazio, G. R., Davidson, M. T., and Cowan, D. R. (2009). "Barge bow force-deformation relationships for barge-bridge collision analysis." *Transp. Res. Rec.*, **2131**, 3–14.
- Cowan, D. R. (2007). "Development of time-history and response spectrum analysis procedures for determining bridge response to barge impact loading." Ph.D. thesis, Univ. of Florida, Gainesville, FL.
- Cowan, D. R., Consolazio, G. R., and Davidson, M. T. (2015). "Response-spectrum analysis for barge impacts on bridge structures." *J. Bridge Eng.*, **10.1061/(ASCE)BE.1943-5592.0000772**, 04015017.
- Cowper, G. R., and Symonds, P. S. (1957). "Strain hardening and strain rate effects in the impact loading of cantilever beams." *Technical Rep. No. 28*, Brown Univ., Providence, RI.
- Davidson, M. T., Consolazio, G. R., and Getter, D. J. (2010). "Dynamic amplification of pier column internal forces due to barge-bridge collision." *Transp. Res. Rec.*, **2172**, 11–22.
- Davidson, M. T., Consolazio, G. R., Getter, D. J., and Shah, F. D. (2013). "Probability of collapse expression for bridges subject to barge collision." *J. Bridge Eng.*, **10.1061/(ASCE)BE.1943-5592.0000376**, 287–296.
- Fan, W., and Yuan, W. (2012). "Shock spectrum analysis method for dynamic demand of bridge structures subjected to barge collisions." *Comput. Struct.*, **90–91**, 1–12.
- FB-MultiPier [Computer software]. Bridge Software Institute, Univ. of Florida, Gainesville, FL.
- FHWA (Federal Highway Administration). (2004). "Manual for LS-DYNA soil material model 147." *FHWA-HRT-04-095*, U.S. Dept. of Transportation, Washington, DC.
- Fujikake, K., Li, B., and Soeun, S. (2009). "Impact response of reinforced concrete beam and its analytical evaluation." *J. Struct. Eng.*, **10.1061/(ASCE)ST.1943-541X.0000039**, 938–950.
- Harik, I. E., Shaaban, A. M., Gesund, H., Valli, G. Y. S., and Wang, S. T. (1990). "United States bridge failures, 1951–1988." *J. Perform. Constr. Facil.*, **10.1061/(ASCE)0887-3828(1990)4:4(272)**, 272–277.
- He, K. Q., and Zhang, Y. Z. (2008). "Detection and data analysis of the collapsed part of Jiuliang Bridge under water." *Pearl River Water Transp.*, **3**, 50–53 (in Chinese).
- Jiang, H. (2011). "Research on the damage of bridge structure with high piles in deep waterway caused by vessel collision based on the numerical methods." Ph.D. thesis, Tongji Univ., Shanghai, China (in Chinese).
- Jiang, H., and Chorzepa, M. G. (2015a). "Evaluation of a new FRP fender system for bridge pier protection against vessel collision." *J. Bridge Eng.*, **10.1061/(ASCE)BE.1943-5592.0000658**, 05014010.
- Jiang, H., and Chorzepa, M. G. (2015b). "An effective numerical simulation methodology to predict the impact response of pre-stressed concrete members." *Eng. Fail. Anal.*, **55**, 63–78.
- Jiang, H., and Chorzepa, M. G. (2016). "Case study: Evaluation of a floating steel fender system for bridge pier protection against vessel collision." *J. Bridge Eng.*, **10.1061/(ASCE)BE.1943-5592.0000947**, 05016008.
- Jiang, H., Wang, J. J., and He, S. H. (2012a). "Numerical simulation on continuous collapse of reinforced concrete girder bridge subjected to vessel collision." *J. Vib. Shock*, **31**(10), 68–73 (in Chinese).
- Jiang, H., Wang, X. W., and He, S. H. (2012b). "Numerical simulation of impact tests on reinforced concrete beams." *Mater. Des.*, **39**, 111–120.
- Jiang, H., and Zhao, J. D. (2015). "Calibration of the continuous surface cap model for concrete." *Finite Elem. Anal. Des.*, **97**, 1–19.
- Jones, N. (1989). *Structural impact*, Cambridge University Press, Cambridge, U.K.
- Kelly, J. (2011). "The effects of impact loading on prestressed concrete beams." Ph.D. thesis, Heriot-Watt Univ., Edinburgh, Scotland.
- LS-DYNA 971 [Computer software]. Livermore Software Technology Corporation, Livermore, CA.
- LSTC (Livermore Software Technology Corporation). (2010). *LS-DYNA keyword user's manual ver. 971*, Livermore, CA.

- LSTC (Livermore Software Technology Corporation). (2015). *LS-DYNA theoretical manual*, Livermore, CA.
- McVay, M. C., Wasman, S. J., Consolazio, G. R., Bullock, P. J., Cowan, D. R., and Bollmann, H. T. (2009). "Dynamic soil-structure interaction of bridge substructure subject to vessel impact." *J. Bridge Eng.*, **10**.1061/(ASCE)1084-0702(2009)14:1(7), 7–16.
- Ministry of Transport of the P.R.C. (2004). "Code for design of highway reinforced concrete and prestressed concrete bridges and culverts." *JTG D62-2004*, Beijing.
- People.cn. (2007). "The collapse of the Guangdong Jiujiang Bridge resulted from a vessel collision." (<http://society.people.com.cn/GB/8217/86231/index.html>) (Aug. 1, 2016).
- Sha, Y. Y., and Hao, H. (2013a). "Laboratory tests and numerical simulations of barge impact on circular reinforced concrete piers." *Eng. Struct.*, **46**, 593–605.
- Sha, Y. Y., and Hao, H. (2013b). "Numerical simulation of barge impact on a continuous girder bridge and bridge." *Int. J. Protective Struct.*, **4**(1), 79–96.
- Wang, J. J., and Jiang, H. (2011). "Quasi-static analysis of anti-collision capacity of high piers embedded in rock under deep water." *J. Disaster Prev. Mitigation Eng.*, **31**(2), 131–137 (in Chinese).
- Yuan, P., and Harik, I. E. (2008). "One-dimensional model for multi-barge flotillas impacting bridge piers." *Comput.-Aided Civ. Infrastruct. Eng.*, **23**(6), 437–447.